Introducing the Concept of Potential-Based Organ Contours

Janine Becker and Mattia Fedrigo

***Abstract*—The aim of this paper is to explore a new method for organ contour description in radiology and radiation protection. The method bases on the mathematical computation of electrical fields, exploited are the equipotential lines caused by a potential field of a distribution of point sources in analogy to electric charges. The organ shape is described by the potential values of the field, the contour by the equipotentials. The potential-dependent methods offers an inside–outside criterion and can be scaled in size and edited by changing the source points. Because of that it offers a flexible possible framework for organ contour editing and also toward segmentation. The main focus of this paper is the proof of principle, i.e., the optimization of the source point coordinates and source strengths, to show the transfer of voxelized organ borders to potential-based contours. The already voxelized organ borders were from a human voxel phantom generated from 2-D CT images of a real patient. Results for several closed and compact organs shall be presented and the limitations, future applications and possibilities addressed, e.g., the advantages of an implementation in Monte Carlo calculations of radiation transport.**

***Index Terms*—Equipotential contour, organ modeling, potential-based contour.**

I. Introduction

A NUMERICAL description (modeling) of human anatomy is necessary for various fields of application, like operation simulation, e.g., [1], and simulation of irradiations by ionizing or nonionizing radiation, e.g., [2]–[5]. For the calculation of organ doses in radiation protection human phantoms [2], [6]–[12] and their modeled organs are essential. The organ dose $D_{\text{org}} = \Delta E/\Delta m$ is defined by the energy ΔE deposited by the radiation in an organ of mass Δm and therefore not directly measurable. In order to obtain these organ doses the radiation transport is simulated by Monte Carlo codes. For a Monte Carlo simulation of radiation transport the history of photons or particles is followed. At the points of their interactions and endpoints the released energy is assigned to the whole organ. Here, the spatial information of the organ is needed to calculate the respective dose conversion coefficients. For simulation beyond that it would be desirable to implement additional information about, e.g., mechanical, electrical metabolic, or inflammatory status [13].

Natural forms tend to be smooth and closed, compact organs like heart and stomach can be seen as globally convex closed shapes. The equipotential lines of a potential field seem to match this aspect. They are continuous and closed. The potential-based method is an indirect but continuous delineation of the organ border by source points. The potential field describes the organ border by equipotential lines. By specifying a potential range walled and thin organs can be described, e.g., the periosteum or the skin [14]. The gradient of the field provides information if a point is inside or outside of the shape. This is a key function in terms of Monte Carlo simulation of radiation transport. The set of source points, the source strengths and one potential value for an organ contour is an effective data compression and provides a memory saving way of storage and editing by no loss on information.

The aim of this paper has been to develop a practicable method to identify the distribution of source points, whose equipotential surface closely approximates a given organ surface. At the present stage, the focus will be on the approximation of organ contours in the 2-D case, and the feasibility of the new approach will be tested for the case that all source strengths have positive values.

II. State of the Art

So-called voxel models [5]–[12], [15] have been proven to be adequate for radiation transport simulation. They consist of a 3-D matrix of voxels with different organ identification numbers as classification system. Many such models are presently available. They offer more anatomic reality than purely mathematical models describing organs by mathematical expressions [16]–[18]. The resolution of the voxels plays a big role. This feature mainly dictates the smoothness of the organ surface and how realistic an organ can be represented. Small or thin tissues under voxel resolution cannot be delineated or are overestimated in weight and volume, e.g., skin and walled organs. A higher resolution is beneficial for the realistic delineation of organs but affects the calculation time on the other hand. In recent years interest has turned toward individual modeling of organs needed for personal dosimetry, patient treatment or medical image simulation, creating new demands concerning the adjustment of existing models and of the spatial resolution. Since the effort of segmenting new organ models from medical images is still higher than their editing in size or form, the main focus has been on their adaptation to given specifications. Furthermore, the modeling of actual

Manuscript received December 19, 2017; revised February 26, 2018; accepted April 2, 2018. *(Corresponding author: Janine Becker.)*

J. Becker is with the Helmholtz Center Munich, Institute of Radiation Protection, 85764 Neuherberg, Germany (e-mail: janine.becker@helmholtz-muenchen.de).

M. Fedrigo was with the Helmholtz Center Munich, AMSD—Research Unit Medical Radiation Physics and Diagnostics, Munich, Germany.

Color versions of one or more of the figures in this paper are available online at http://ieeexplore.ieee.org.

Digital Object Identifier 10.1109/TRPMS.2018.2829266

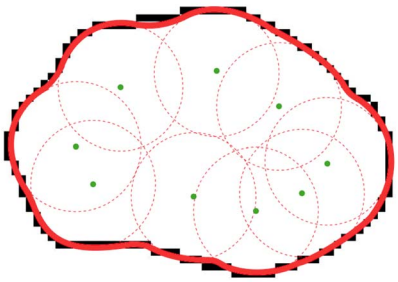

Fig. 1. Source points (green), equipotential lines of the single sources (dashed circles), and common, equipotential line (red) for organ contour (black).

patient data is of interest for operation planning and training, as well as for radiation therapy planning and organ dose calculation for diagnostic radiation exposures. Moreover, the editing of the organs and tissues on voxel base is very laborious [19]. Another way to scale organs in size and edit their shape is the transfer into other representations like hybrid representations, e.g., [20]–[24] or polygonal nets and nonuniform rational B-splines (NURBS) [25]. NURBS are a generalization of B-splines and Bézier curves and surfaces, which are fitted to control points on the contour or surface. These methods describe only the contour and do not hold additional information.

The transfer from one representation into another is usually done by manual interaction on a graphical user interface of available software, e.g., Rhinoceros [26].

In the following other modeling methods that have been introduced in the literature are described. M-reps [27] have been developed to represent biological forms. Here, medial atoms on a line build the objects. A hierarchy of figures builds the resulting shape. They do not offer a classification method, meaning an individual atom or shape is assigned to a tissue. In operation planning a sphere-filled organ modeling [28] can be found. This representation is close to voxels. But depending on the modeled anatomy, it is probably memory intense as no spheres inside an area can be omitted. Furthermore, it is possible to model single organ shapes via Fourier surfaces [29], spherical harmonics [30]–[32], and wavelets [33], [34]. These methods are not available in common software and have to be implemented by the user. They are based on a set of parameters and are not editable in a straightforward way via graphical interaction and require a specialist for applying. Further mathematical descriptions mainly describing the contour of an organ can be found in [35]–[38]. These approaches are commonly used for segmentation, i.e., organ extraction from medical images; to the authors' knowledge they are not used as input format for the simulation of radiation transport.

III. Conceptual Basics

For a single source point, analogous to an electric charge, the 3-D potential field in a homogeneous medium is a sphere, and if cut by any plane, the equipotential lines are circles. For a group of source points the superposition principle works, and the resulting equipotential line will form a more detailed contour, see Figs. 1 and 2.

It shall be analyzed if this idea can be put in praxis, and how the source points can be distributed to obtain a resulting

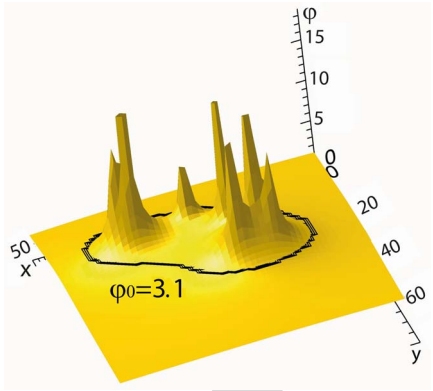

Fig. 2. Potential field with 7 Q, i.e., the peaks the potential field, and equipotential line (black) with $\varphi_0 = 3.1$ for a stomach contour, see also Fig. 11.

equipotential line that is closely tracing a given realistic organ contour.

A. Source Points With (Q/r)-Potential

For a better understanding how the source points can lead to a contour a short derivation of the underlying electric field principle is presented here

$$\vec{E} = \frac{Q}{4\pi\varepsilon r^2}\vec{e}_r. \tag{1}$$

Formula (1) shows the electrical field strength $\vec{E}$ of an electrical point charge Q in a medium with the dielectric constant ε at a distance r. The associated electrical potential φ is

$$\varphi = \frac{Q}{4\pi\varepsilon r}. \tag{2}$$

For a distribution of z point charges the resulting electrical potential φ is obtained according to the superposition principle

$$\varphi = \sum_{i=0}^{z} \frac{Q_i}{4\pi\varepsilon r_i}. \tag{3}$$

In order to model the organ surfaces and no actual physical situation we use a mathematical analogy: we consider source points instead of electrical point charges. The physical constant ε is neglected, a "source strength" Q_i is associated with each source point i resulting in a sum potential φ. We define that Q_i is a positive number and r is the distance from the point source. The potential for a spatial distribution of z source points is

$$\varphi = \sum_{i=0}^{z} \frac{Q_i}{r_i}. \tag{4}$$

B. Computation and Display of the Potential-Based Lines

To show a line of equipotentials it is necessary to pick a field point and compare its local potential φ_0 to the rest of the potential field. It is the question how to decide for this point of reference. To answer this question the inertia axes of the organ slice were utilized.

The axes of inertia span a coordinate system with their origin in the barycenter B of the organ slice, as shown in Fig. 3. The axes cut the organ borders and the intersection points serve as reference for the potential. In the process

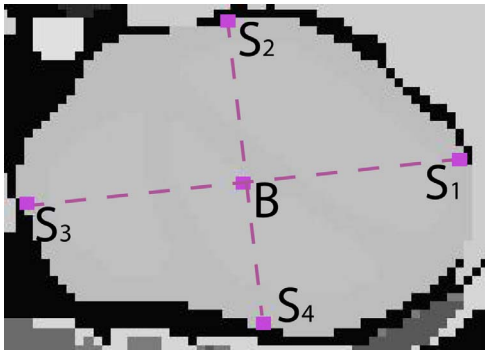

Fig. 3. Transversal voxelized slice of the heart with barycenter B and intersection points $S_{1...4}$ of the inertia axes and organ border.

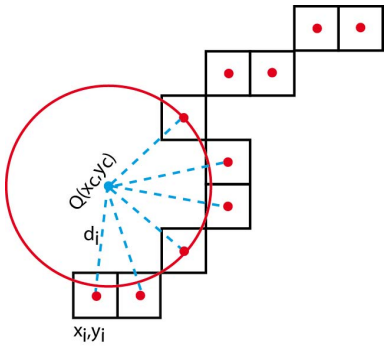

Fig. 4. Computation of source point coordinates x_c, y_c by circle approximation of x_j, y_j.

of first implementation the potential-based contours for all four intersection points $S_{1...4}$ were displayed and compared. The resulting potential-based contours are slightly different and shall be compared by parameters of goodness, see Section III-E.

C. Positioning of the Source Points

After the consideration how to adapt the basic idea and how to display a potential-based contour there is still the open question how many and where to place source points in a sensible way to proof the concept.

The already known organ border of a voxelized computational phantom shall serve as a guideline for the potential-based contours. The voxel model "Laura" [39] of the HMGU voxel model family [6] provided the organ borders that were transformed in potential-based contours. The so-called voxelized phantoms offer a realistic presentation of human anatomy. Here, it can be seen if the method of a source point distribution fits for realistic organ shapes. In essence every other phantom of [6] or set of contour coordinates could be used.

1) Coordinates of the Source Points: An iteration process shall distribute a number of sources within the given organ border. The individual source points have to be placed in regard to their respective border segment, which is obtained by dividing the total number of border voxels by the total number of sources. Since the equipotential line of a single source point is a circle in 2-D (see Section III, Fig. 1), it is assumed the respective border voxels x_j, y_j are on this circle and the source is placed at its center point x_c, y_c at a the radius r.

Formula (5) describes the variation of the center point coordinates and its distance to each border voxel x_j, y_j by means of auxiliary variables ϑ, η, ρ

$$(x_c, y_c, r) = \underset{\vartheta,\eta,\rho}{\operatorname{argmin}} \sum_{j=1}^{n} \left[\left(x_j - \vartheta\right)^2 + \left(y_j - \eta\right)^2 - \rho^2 \right]^2. \quad (5)$$

This algorithm serves to minimize the sum of the squared differences $(d_j^2 - r^2)^2$, where

$$d_j^2 = \left(x_j - x_c\right)^2 + \left(y_j - y_c\right)^2. \quad (6)$$

These expressions were the basis for a system of equations whose final matrix formulation was solved via Cramers' rule and thus provided the desired center points x_c, y_c.

D. Choice of the Source Strengths

After the source points Q_i have been placed in a distance r to the border, the source strengths are determined by

$$Q_i = r_i \cdot \varphi_R \quad (7)$$

where the potential on the border is $\varphi_R = 1$. The sum potential on the organ border φ_0 will differ from 1 because of the superposition of all point sources. It is expected to be higher but remaining within the same order of magnitude. Among all tried ways this simple one provided adequate results.

E. Comparison of the Potential-Based Organ Area With Voxel Area

After placing the source points and displaying the equipotential line there must be a way of judging how well the final potential-based contour matches the voxelized one. For this purpose the parameters of goodness are introduced.

1) Parameters for the Goodness of Fit: For the comparison of the equipotential with the voxel representation, the overlap U between the potential-modeled and originally voxelized organ region is computed. The combined area of voxelized (O) and potential-based (M) organ region except the intersection of both is related to the original region (O) by

$$U = \frac{O \cup M \setminus O \cap M}{O}. \quad (8)$$

This can be intuitively understood as organ area not covered by the potential-based region. The closer to zero the better the match between the areas. Because one goodness-of-fit parameter did not turn out to be sufficient, the distance a between the barycenters of original and potential-based contour were additionally calculated

$$a = \sqrt{(x_O - x_M)^2 + (y_O - y_M)^2}. \quad (9)$$

Formula (9) subtracts the coordinates (x_O, y_O) and (x_M, y_M) of the barycenters of the original and modeled area and a is given in voxel distances. The optimal case is when there is no distance between the barycenters, i.e., the expression is zero.

The values U and a are calculated for a source point distribution, the pair with the smallest values, i.e., closest to zero, indicates the best fit. This way resulting potential-based contours can be compared and evaluated.

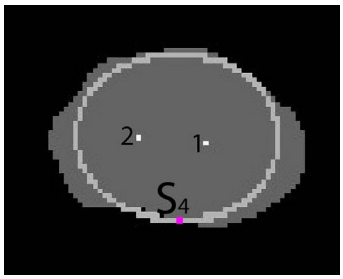

Fig. 5. Voxelized heart slice (dark gray) with potential-based contour (light gray) of 2Q, U=0.05, a=0.44, S_4.

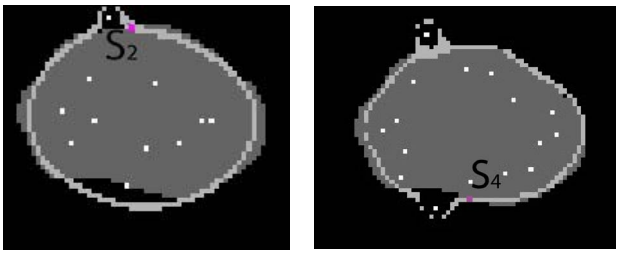

Fig. 6. Heart with 11Q (U=0.04, a=1.13, left) and 16 Q(U=0.04, $a = 0.71$, right).

IV. Results

The transversal slice T256 of the voxel data set Laura provided the heart contour that served for testing the new method, see Figs. 5–7. After the evaluation of the first trials, the positioning of the source points, see Section IV-B, was refined and applied for organ slices of heart, bladder, stomach, and aorta, as presented in Section IV-C.

A. First Trials

For the heart slice, the number of source points was varied from 2 to 42. The parameters of goodness U and a were analyzed for every distribution at the four intersection points S_1, S_2, S_3, or S_4 between the axes of inertia and the organ border. Table I shows an excerpt of the parameters for the iteration process. The full table can be found in [40].

For just two source points, Fig. 5 shows that the principle of superposition is working. Exact tracing of the organ contour is not yet achieved, but that a match between the equipotential line and the organ border appears as possible, when the number of source points is increased. The distributions with 11 sources (Fig. 6, left) and 16 sources (Fig. 6, right) show the best parameters of all distributions. For both approximations small areas outside the original organ contour have been modeled, this is due to the more concave segment of the organ contour, the single source was oriented to.

In the example of Fig. 7 the probable optimal number of source points is exceeded. Ring structures were created rather than a closed area.

B. Conclusion for Source Point Positioning

From these results the following conclusions have been deduced.

1) The algorithm for minimization the goodness-of-fit parameters does not have an unique solution. For one organ contour several source point distributions with nearly the same set of goodness parameters have been found.
2) Highly curved contours benefit from a higher number of source points.

The following rules for numerical stability were adopted in the placing algorithm.

1) In a distribution with source points of the same sign, the source points have to be placed inside the organ region.
2) Source points very close to or on the organ border lead to numerical instabilities. Improvements may be achieved by eliminating unfavorable source points.

TABLE I
Iterations of 9–18 Source Points Q, With the Goodness-of-Fit Parameters U and a for the Intersection Points S_1 to S_4

Q Number	S_i	U	a
9	S_1	0.05	1.47
9	S_2	0.05	1.65
9	S_3	0.07	1.31
9	S_4	0.07	2.25
10	S_1	0.05	1.97
10	S_2	0.05	1.99
10	S_3	0.05	2.14
10	S_4	0.1	2.36
11	S_1	0.06	1.19
11	S_2	0.04	1.13
11	S_3	0.05	1.18
11	S_4	0.09	1.09
12	S_1	0.08	8.27
12	S_2	0.08	7.32
12	S_3	0.1	9.02
12	S_4	0.13	8.76
13	S_1	0.07	3.59
13	S_2	0.08	3.34
13	S_3	0.1	3.13
13	S_4	0.08	3.81
14	S_1	0.07	2.07
14	S_2	0.07	2.26
14	S_3	0.1	2.3
14	S_4	0.09	3.23
15	S_1	0.07	8.35
15	S_2	0.06	7.92
15	S_3	0.07	8.22
15	S_4	0.06	7.33
16	S_1	0.04	1.3
16	S_2	0.04	0.96
16	S_3	0.05	0.24
16	S_4	0.04	0.71
17	S_1	0.04	4.21
17	S_2	0.04	4.73
17	S_3	0.05	4.54
17	S_4	0.05	5.02
18	S_1	0.13	4.28
18	S_2	0.07	4.99
18	S_3	0.08	4.95
18	S_4	0.09	5.44

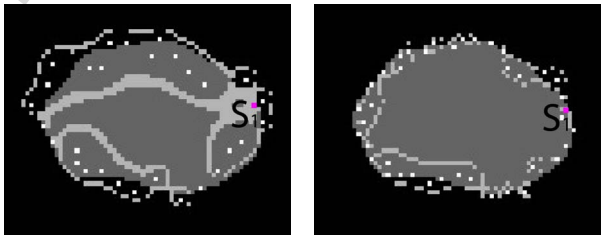

Fig. 7. Heart T256 with 29 Q ($U = 0.18$, $a = 1.02$, left) and 39 Q (U=0.24 a=0.75, right) each for S_1.

C. Potential-Based Organ Contour

Based on this experience, potential-based contours for slices of heart, aorta, kidney, stomach, and bladder have

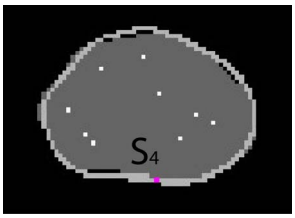

Fig. 8. Heart slice T256, 9 Q, $U = 0.02$, and $a = 0.29$ for S_4.

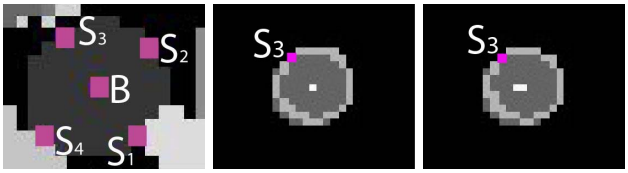

Fig. 9. Voxelized slice of aorta with barycenter B and intersections points $S_{1...4}$ (left) and potential-based contours with $1Q$ (middle) and $2Q$ (right), both $U = 0.04$, $a = 0.02$ for S_3.

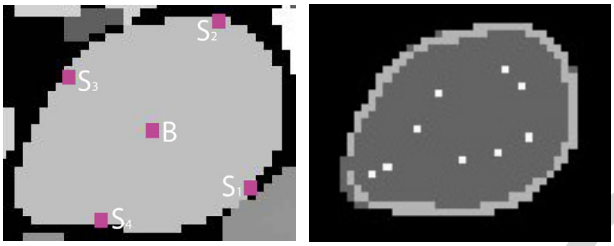

Fig. 10. Voxelized kidney slice with barycenter B and intersections points$S_{1...4}$ (left) and $9Q$, $U = 0.01$, and $a = 0.55$ for S_1 (right).

been generated. The source points were distributed within the organ region but neither close nor on the organ border according to the numerical stability rules of the placing algorithm.

Figs. 8–12 present the original voxelized slices together with the best source point distributions with their respective goodness parameters. The area within and including the potential-based contour can be understood as organ area.

1) Heart, Aorta, and Kidney: After the implementation of the restrictions for placing the sources a distribution of nine sources provided the best fit of the potential and voxel-based contour for the heart slice (Fig. 8).

For the aorta the distribution of one and two source points worked the same because of its nearly circular shape. For radiation protection purposed the aorta is not divided in wall and blood volume.

The best set of parameters of all organs has been achieved for the kidney (Fig. 10). Only very few voxels were found outside the equipotential line.

2) Walled Organs: In the underlying voxel data of stomach (Fig. 11) and bladder (Fig. 12) consist of wall and content. Here, the content provided the coordinates for the source point placement.

In the upper part of Fig. 11 the equipotential line of seven source points covers a small area outside the organ.

Similar to the stomach, the bladder (Fig. 12) is divided in wall and content. Here, too the content was taken as basis for the source point placements.

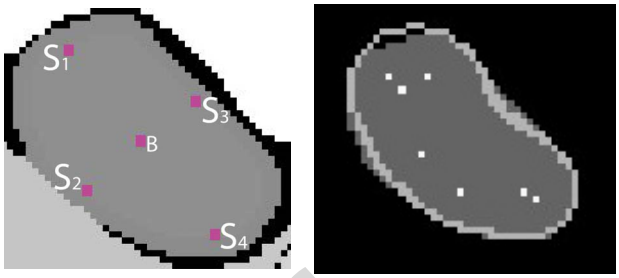

Fig. 11. Stomach T250, B and $S_1..S_4$ (left); $7Q$, $U = 0.02$, and $a = 0.21$ for S_4 (right).

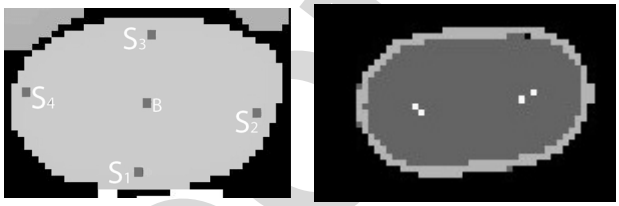

Fig. 12. Bladder T185, B, and $S_{1...4}$ (left); 4 Q, $U = 0.02$, and $a = 0.27$ for S_1 (right).

V. Discussion of Potential-Based Features

Figs. 8–12 give proof the principle of source points works and show that a satisfying quality of modeling is achieved; even slightly concave contours were modeled by the proper choice of source distances.

A. Data Compression

For saving a continuous contour the coordinates of the source points and the potential value at the respective reference point are needed, for the given examples it was less than 12 numbers. The calculation time for obtaining a distribution for a given number of source points is in the range of a few seconds.

B. Data Input for Source Point Placing

Since the data for the center calculations are coordinates, the algorithm works for coronal, sagittal, and transversal slices. The results of Section IV were obtained by implementing the voxel model Laura [39]. The method can be applied also to other voxel phantoms. To demonstrate this, heart contours of the human phantoms Golem (T55 $U = 0.02$, $a = 0.13$) and Irene (T255 $U = 0.02$, $a = 0.55$) were modeled. In theory also other boundary representations, such as polygon meshes, could deliver the basis coordinates for positioning the source points as long as the boundary contour can be approximated by circles (2-D) or spheres (3-D).

C. Scaling

A potential-based organ contour can be easily scaled in size. It is sufficient to multiply the coordinates of the source points as well as their source strengths Q_i by a factor s. For the enlarged heart region, shown in Fig. 13, a factor $s = 1.4$ was

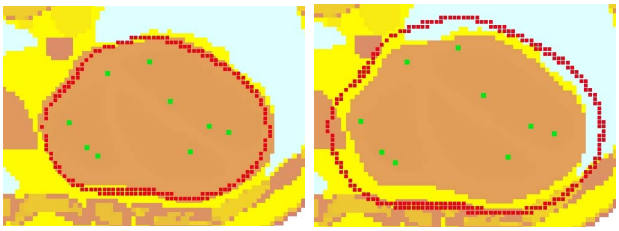

Fig. 13. Scaling of the equipotential line $\varphi_0 = 4.13$ (red) in the heart slice T256 (brown).

chosen arbitrarily

$$\varphi_{\mathbf{0}} = \sum_{i=0}^{z} \frac{sQ_i}{sr_i} = \sum_{i=0}^{z} \frac{Q_i}{r_i}. \tag{10}$$

Although all coordinates will be subjected to this affine transformation, the potential φ_0 on the equipotential line will be conserved.

This feature is of interest when existing organ model have to be adapted to individual shapes of a patient. For this purpose also a change of place and source strength of the single sources is of interest if a rigid transformation is not sufficient. At the moment this feature works only manually.

D. Walled Organs and Subtissue

It is possible to describe the organ wall as a potential range, e.g., $\varphi_{\text{wall}} = \varphi_0 \pm \Delta\varphi$. For subtissues inside an organ a range of potential values could be utilized. In a voxel model all voxel adjacent to another tissue make the organ border. It is straightforward that the resolution of the voxels influence the resulting thickness of the wall. In this case Laura provides voxels of $1.875 * 1.875 * 5$ mm^3 which makes it difficult to present walled or thin organs in a accurate way.

E. In- or Outside Criterion of the Potential-Based Contour

For a Monte Carlo simulation of radiation transport the released energy of an interaction has to be assigned to an organ volume. In case of a voxelized human phantom the organ identification number of a specific voxel informs about the tissue type. In case of boundary representations like polygon meshes and NURBS there is no according information. It is possible to implement these type of phantoms to Monte Carlo code but it is computational intense [41]. Additional algorithms deliver spatial information for assigning the released energy to the correct corresponding tissue, i.e., within which organ contour energy loss happens, [42].

The equipotential line is a closed continuous contour, suitable for compact organs like heart, bladder, or stomach, whose surfaces primarily show convex regions. To check where an arbitrary point is situated in respect to the organ border, it is sufficient to see if $\varphi > \varphi_0$ for being inside or $\varphi < \varphi_0$ for being outside. Further studies are necessary to show if the potential values and the gradient of the potential field provide the expected benefits.

VI. Conclusion

The first trials of the newly explored method of potential-based organ contours look promising and provide further aspects for development. The organ contours were modeled by a source point distribution with an $(1/r)$-potential. This physical approach offers an advantage by making use of the inherent features of the physical quantities and the connections among each other. This way a potential-based delineation provides more information about the organ shape despite basing on a small data set. It offers a flexible frame for delineate natural contours. Depending on the complexity of the organ, a point source might not provide an adequate field geometry. Further studies with other sources, e.g., a line source, would be needed. The regulation of the individual source strengths is a complex issue. The alteration of a single source strength is affecting the whole field and changes the resulting equipotential line.

The focus of this paper was on compact mostly convex organ shapes in 2-D to proof the principle. For small concave parts of organ contours have been satisfactorily modeled by proper spacing between positive sources. The developed placing algorithm is rather basic and does not deliver satisfying results for organ contours with more convex parts or peaks, e.g., tips of the lungs. These parts would benefit from negative sources.

The proposed method can further be used for the extraction of organs from medical images, i.e., for their segmentation. Therefore, a first guess of the contour has to be placed into the medical image. This can be done either manually by placing sources with the mouse or taken from an already voxelized organ border. Here, the implied features of the physical approach are used, i.e., electric force and the field lines of the sources pointing in radial direction away. In combination with an edge detection of the medical image, the field lines of a source and the gradient of the edges are used to tell how well a source point is oriented toward the respective edge. The source points can be shifted individually in a predefined area to a place where the resulting equipotential line traces the edge in a better way. First tests on CT-images with practical results have been made [40].

Outlook

It would be interesting to try more advanced algorithms for source point positioning and the calculation of the source strengths, as well as other potential distributions that may offer mathematical advantages or face special needs for contouring. The implementation of negative source points is an aspects which should be addressed. Concave sections of the organ border would benefit from the use of negative sources.

The implementation of the potential-based method into Monte Carlo simulations of radiation transport is considered possible, see Section V-E. Small and thin walled organs could be represented which have not been included in Monte Carlo code until now. The point of data compression is also interesting in regard to the computationally intense simulation of radiation transport. Therefor, a 3-D representation with sources is necessary. Equations (5) and (6) were also extended to 3-D but not yet implemented. The compact data structure of the potential-based organ contours also appears applicable in computer assisted diagnosis and growth modeling for tumors, e.g., in brains or tumor or organ tracking in radiation therapy.

ACKNOWLEDGMENT

The authors would like to thank the Technische Universität Ilmenau and the Helmholtz Zentrum München, especially Prof. A. Keller and Prof. D. Regulla, for the possibility to do this paper and the provided support. Furthermore, the authors would also like to express my sincere gratitude to my advisor Prof. D. Harder, Universität Göttingen, for his support and guidance.

REFERENCES

[1] M. Bro-Nielsen, "Finite element modeling in surgery simulation," *Proc. IEEE*, vol. 86, no. 3, pp. 490–503, Mar. 1998.

[2] T. Nagaoka *et al.*, "Development of realistic high-resolution whole-body voxel models of Japanese adult males and females of average height and weight, and application of models to radio-frequency electromagnetic-field dosimetry," *Phys. Med. Biologie*, vol. 49, no. 1, pp. 1–15, 2004.

[3] P. Dimbylow, "Development of the female voxel phantom, NAOMI, and its application to calculations of induced current densities and electric fields from applied low frequency magnetic and electric fields," *Phys. Med. Biol.*, vol. 50, no. 6, pp. 1047–1070, 2005.

[4] M. Clemens *et al.*, "Bioelectromagnetic field simulations using high-resolution human anatomy models with the finite integration technique," *J. RF Eng. Telecommun.*, vol. 63, nos. 7–8, pp. 163–167, 2009.

[5] W. Bolch, C. Lee, M. Wayson, and P. Johnson, "Hybrid computational phantoms for medical dose reconstruction," *Radiat. Environ. Biophys.*, vol. 49, no. 2, pp. 155–168, 2010.

[6] N. Petoussi-Henss, M. Zankl, U. Fill, and D. Regulla, "The GSF family of voxel phantoms," *Phys. Med. Biol.*, vol. 47, no. 1, pp. 89–106, 2002.

[7] R. Kramer, J. W. Vieira, H. J. Khoury, F. R. A. Lima, and D. Fuelle, "All about MAX: A male adult voxel phantom for Monte Carlo calculations in radiation protection dosimetry," *Phys. Med. Biol.*, vol. 48, no. 10, pp. 1239–1262, 2003.

[8] R. Kramer *et al.*, "All about FAX: A female adult voxel phantom for Monte Carlo calculation in radiation protection dosimetry," *Phys. Med. Biol.*, vol. 49, no. 23, pp. 5203–5216, 2004.

[9] C. Y. Shi and X. G. Xu, "Development of a 30-week-pregnant female tomographic model from computed tomography (CT) images for Monte Carlo organ dose calculations," *Med. Phys.*, vol. 31, no. 9, pp. 2491–2497, 2004.

[10] S. Park, J. K. Lee, and C. Lee, "Development of a Korean adult male computational phantom for internal dosimetry calculation," *Radiat. Protect. Dosimetry*, vol. 121, no. 3, pp. 257–264, 2006.

[11] K. Sato, H. Noguchi, Y. Emoto, S. Koga, and K. Saito, "Japanese adult male voxel phantom constructed on the basis of CT images," *Radiat. Protect. Dosimetry*, vol. 123, no. 3, pp. 337–344, 2007.

[12] B. Zhang, J. Ma, L. Liu, and J. Cheng, "CNMAN: A Chinese adult male voxel phantom constructed from color photographs of a visible anatomical data set," *Radiat. Protect. Dosimetry*, vol. 124, no. 2, pp. 130–136, 2007.

[13] B. He *et al.*, "Grand challenges in interfacing engineering with life sciences and medicine," *IEEE Trans. Biomed. Eng.*, vol. 60, no. 3, pp. 589–598, Mar. 2013.

[14] F. Spiers, "Transition-zone doesimetry," in *Radiation Protection Dosimetry*, F. H. Attix and E. Tochilin, Eds., vol. 3. New York, NY, USA: Academic Press, 1968, pp. 809–867.

[15] "Adult reference computational phantoms," *Ann. ICRP*, vol. 39, no. 2, pp. 1–2, 2009.

[16] H. L. Fisher and W. S. Snyder, "Distribution of dose in the body from a source of gamma rays distributed uniformly in an organ," Oak Ridge Nat. Lab., Oak Ridge, TN, USA, Rep. ORNL 4168, 1967.

[17] R. Kramer, M. Zankl, G. Williams, and G. Drexler, "The calculation of dose from external photon exposures using reference human phantoms and Monte Carlo methods, part I: The male (Adam) and female (Eva) adult mathematical phantoms," GSF-Nat. Res. Center Environ. Health, Rep. GSF S-885, 1982.

[18] M. Cristy and K. F. Eckerman, "Specific absorbed fractions of energy at various ages from internal photon sources," Oak Ridge Nat. Lab., Oak Ridge, TN, USA, Rep. ORNL TM-8381, 1987.

[19] J. Becker, M. Zankl, and N. Petoussi-Henss, "A software tool for modification of human voxel models used for application in radiation protection," *Phys. Med. Biol.*, vol. 52, no. 9, pp. 195–205, 2007.

[20] X. G. Xu, V. Taranenko, J. Zhang, and C. Shi, "A boundary-representation method for designing whole-body radiation dosimetry models: Pregnant females at the ends of three gestational periods—RPI-P3, -P6 and -P9," *Phys. Med. Biol.*, vol. 52, no. 23, pp. 7023–7044, 2007.

[21] C. Lee, C. Lee, S.-H. Park, and J.-K. Lee, "Development of the two Korean adult tomographic computational phantoms for organ dosimetry," *Med. Phys.*, vol. 33, no. 2, pp. 380–390, 2006.

[22] C. Lee *et al.*, "The UF family of reference hybrid phantoms for computational radiation dosimetry," *Phys. Med. Biol.*, vol. 55, no. 2, pp. 339–363, 2010.

[23] J. Bond *et al.*, "Series of 4D adult XCAT phantoms for imaging research and dosimetry," in *Proc. SPIE*, vol. 8313, 2012, Art. no. 83130P.

[24] C. H. Kim *et al.*, "The reference phantoms: Voxel vs polygon," *Ann. ICRP*, vol. 45, no. S1, pp. 188–201, 2016.

[25] B. Tsagaan, A. Shimizu, H. Kobatake, and K. Miyakawa, *An Automated Segmentation Method of Kidney Using Statistical Information* (Lecture Notes in Computer Science), vol. 2488. Heidelberg, Germany: Springer, 2002, pp. 556–563, doi: 10.1007/3-540-45786-0_69.

[26] (2015). *Rhinoceros—NURBS Modeling Für Windows, Version 4 SR9, 9-March-2011 Commercial*. [Online]. Available: https://www.flexicad.com/

[27] H. Blum, "Biological shape and visual science (part I)," *J. Theor. Biol.*, vol. 38, no. 2, pp. 205–287, 1973.

[28] S. Suzuki, N. Suzuki, A. Hattori, A. Uchiyama, and S. Kobayashi, "Sphere-filled organ model for virtual surgery system," *IEEE Trans. Med. Imag.*, vol. 23, no. 6, pp. 714–722, Jun. 2004.

[29] L. H. Staib and J. S. Duncan, "Deformable Fourier models for surface finding in 3-D images," *Visual. Biomed. Comput.*, vol. 1808, pp. 90–104, 1992.

[30] F. Mofrad *et al.*, "Statistical construction of a Japanese male liver phantom for internal radionuclide dosimetry." *Radiat. Protect. Dosimetry*, vol. 141, no. 2, pp. 140–148, 2010.

[31] T. Tateyama *et al.*, "Shape representation of human anatomy using spherical harmonic basis function," in *Proc. 6th Int. Conf. Comput. Sci. Converg. Inf. Technol. (ICCIT)*, 2011, pp. 866–869.

[32] A. Matheny and D. B. Goldgof, "The use of three- and four-dimensional surface harmonics for rigid and nonrigid shape recovery and representation," *IEEE Trans. Pattern Anal. Mach. Intell.*, vol. 17, no. 10, pp. 967–981, Oct. 1995.

[33] C. Davatzikos, X. Tao, and D. Shen, "Hierarchical active shape models, using the wavelet transform," *IEEE Trans. Med. Imag.*, vol. 22, no. 3, pp. 414–423, Mar. 2003.

[34] D. Nain, S. Haker, A. Bobick, and A. Tannenbaum, "Multiscale 3-D shape representation and segmentation using spherical wavelets," *IEEE Trans. Med. Imag.*, vol. 26, no. 4, pp. 598–618, Apr. 2007.

[35] C. Xu and J. L. Prince, "Snakes, shapes, and gradient vector flow," *IEEE Trans. Image Process.*, vol. 7, no. 3, pp. 359–369, Mar. 1998.

[36] T. McInerney and D. Terzopoulos, "A dynamic finite element surface model for segmentation and tracking in multidimensional medical images with application to cardiac 4D image analysis," *Comput. Med. Imag. Graph.*, vol. 19, no. 1, pp. 69–83, 1995.

[37] D. Cremers, M. Rousson, and R. Deriche, "A review of statistical approaches to level set segmentation: Integrating color, texture, motion and shape," *Int. J. Comput. Vis.*, vol. 72, no. 2, pp. 195–215, 2007.

[38] T. Heimann and H.-P. Meinzer, "Statistical shape models for 3D medical image segmentation: A review," *Med. Image Anal.*, vol. 13, no. 4, pp. 543–563, 2009.

[39] M. Zankl, K. F. Eckerman, and W. Bolch, "The ICRP reference computational phantoms," *Handbook of Anatomical Models for Radiation Dosimetry*. Boca Raton, FL, USA: Taylor & Francis, 2010, pp. 377–388.

[40] J. Becker, "Beschreibung von organgrenzen als Äquipotentialverlauf finiter quellpunkte mit Q/r-potentialen," Ph.D. Dissertation, Technische Universität Ilmenau, Ilmenau, Germany, 2015.

[41] C. H. Kim, J. J. H. W. Bolch, K. K. Cho, and S. B. Hwang, "A polygon-surface reference Korean male phantom (PSRK-Man) and its direct implementation in Geant4 Monte Carlo simulation," *Phys. Med. Biol.*, vol. 56, no. 10, pp. 3137-3161, 2011.

[42] M. Han *et al.*, "DagSolid: A new Geant4 solid class for fast simulation in polygon-mesh geometry." *Phys. Med. Biol.*, vol. 58, no. 13, pp. 4595–4609, 2013.

AUTHOR QUERIES

AUTHOR PLEASE ANSWER ALL QUERIES

PLEASE NOTE: We cannot accept new source files as corrections for your paper. If possible, please annotate the PDF proof we have sent you with your corrections and upload it via the Author Gateway. Alternatively, you may send us your corrections in list format. You may also upload revised graphics via the Author Gateway.

AQ1: Please provide the postal code for "AMSD—Research Unit Medical Radiation Physics and Diagnostics."
AQ2: Please cite "Fig. 4" inside the text.
AQ3: Please provide the author name for Reference [15].
AQ4: Please provide the organization location for Reference [17].
AQ5: Please confirm if the location and publisher information for Reference [25] is correct as set.
AQ6: Please confirm the volume number for References [23] and [25].
AQ7: Please confirm the volume number and also provide the issue number or month for Reference [29].
AQ8: Please provide the department name for Reference [40].

Introducing the Concept of Potential-Based Organ Contours

Janine Becker and Mattia Fedrigo

***Abstract*—The aim of this paper is to explore a new method for organ contour description in radiology and radiation protection. The method bases on the mathematical computation of electrical fields, exploited are the equipotential lines caused by a potential field of a distribution of point sources in analogy to electric charges. The organ shape is described by the potential values of the field, the contour by the equipotentials. The potential-dependent methods offers an inside–outside criterion and can be scaled in size and edited by changing the source points. Because of that it offers a flexible possible framework for organ contour editing and also toward segmentation. The main focus of this paper is the proof of principle, i.e., the optimization of the source point coordinates and source strengths, to show the transfer of voxelized organ borders to potential-based contours. The already voxelized organ borders were from a human voxel phantom generated from 2-D CT images of a real patient. Results for several closed and compact organs shall be presented and the limitations, future applications and possibilities addressed, e.g., the advantages of an implementation in Monte Carlo calculations of radiation transport.**

***Index Terms*—Equipotential contour, organ modeling, potential-based contour.**

I. Introduction

A NUMERICAL description (modeling) of human anatomy is necessary for various fields of application, like operation simulation, e.g., [1], and simulation of irradiations by ionizing or nonionizing radiation, e.g., [2]–[5]. For the calculation of organ doses in radiation protection human phantoms [2], [6]–[12] and their modeled organs are essential. The organ dose $D_{\text{org}} = \Delta E/\Delta m$ is defined by the energy ΔE deposited by the radiation in an organ of mass Δm and therefore not directly measurable. In order to obtain these organ doses the radiation transport is simulated by Monte Carlo codes. For a Monte Carlo simulation of radiation transport the history of photons or particles is followed. At the points of their interactions and endpoints the released energy is assigned to the whole organ. Here, the spatial information of the organ is needed to calculate the respective dose conversion coefficients. For simulation beyond that it would be desirable to implement additional information about, e.g., mechanical, electrical metabolic, or inflammatory status [13].

Natural forms tend to be smooth and closed, compact organs like heart and stomach can be seen as globally convex closed shapes. The equipotential lines of a potential field seem to match this aspect. They are continuous and closed. The potential-based method is an indirect but continuous delineation of the organ border by source points. The potential field describes the organ border by equipotential lines. By specifying a potential range walled and thin organs can be described, e.g., the periosteum or the skin [14]. The gradient of the field provides information if a point is inside or outside of the shape. This is a key function in terms of Monte Carlo simulation of radiation transport. The set of source points, the source strengths and one potential value for an organ contour is an effective data compression and provides a memory saving way of storage and editing by no loss on information.

The aim of this paper has been to develop a practicable method to identify the distribution of source points, whose equipotential surface closely approximates a given organ surface. At the present stage, the focus will be on the approximation of organ contours in the 2-D case, and the feasibility of the new approach will be tested for the case that all source strengths have positive values.

II. State of the Art

So-called voxel models [5]–[12], [15] have been proven to be adequate for radiation transport simulation. They consist of a 3-D matrix of voxels with different organ identification numbers as classification system. Many such models are presently available. They offer more anatomic reality than purely mathematical models describing organs by mathematical expressions [16]–[18]. The resolution of the voxels plays a big role. This feature mainly dictates the smoothness of the organ surface and how realistic an organ can be represented. Small or thin tissues under voxel resolution cannot be delineated or are overestimated in weight and volume, e.g., skin and walled organs. A higher resolution is beneficial for the realistic delineation of organs but affects the calculation time on the other hand. In recent years interest has turned toward individual modeling of organs needed for personal dosimetry, patient treatment or medical image simulation, creating new demands concerning the adjustment of existing models and of the spatial resolution. Since the effort of segmenting new organ models from medical images is still higher than their editing in size or form, the main focus has been on their adaptation to given specifications. Furthermore, the modeling of actual

Manuscript received December 19, 2017; revised February 26, 2018; accepted April 2, 2018. *(Corresponding author: Janine Becker.)*

J. Becker is with the Helmholtz Center Munich, Institute of Radiation Protection, 85764 Neuherberg, Germany (e-mail: janine.becker@helmholtz-muenchen.de).

M. Fedrigo was with the Helmholtz Center Munich, AMSD—Research Unit Medical Radiation Physics and Diagnostics, Munich, Germany.

Color versions of one or more of the figures in this paper are available online at http://ieeexplore.ieee.org.

Digital Object Identifier 10.1109/TRPMS.2018.2829266

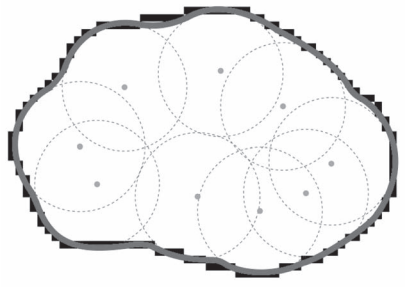

Fig. 1. Source points (green), equipotential lines of the single sources (dashed circles), and common, equipotential line (red) for organ contour (black).

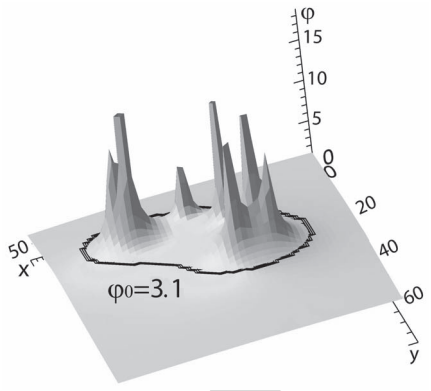

Fig. 2. Potential field with 7 Q, i.e., the peaks the potential field, and equipotential line (black) with $\varphi_0 = 3.1$ for a stomach contour, see also Fig. 11.

patient data is of interest for operation planning and training, as well as for radiation therapy planning and organ dose calculation for diagnostic radiation exposures. Moreover, the editing of the organs and tissues on voxel base is very laborious [19]. Another way to scale organs in size and edit their shape is the transfer into other representations like hybrid representations, e.g., [20]–[24] or polygonal nets and nonuniform rational B-splines (NURBS) [25]. NURBS are a generalization of B-splines and Bézier curves and surfaces, which are fitted to control points on the contour or surface. These methods describe only the contour and do not hold additional information.

The transfer from one representation into another is usually done by manual interaction on a graphical user interface of available software, e.g., Rhinoceros [26].

In the following other modeling methods that have been introduced in the literature are described. M-reps [27] have been developed to represent biological forms. Here, medial atoms on a line build the objects. A hierarchy of figures builds the resulting shape. They do not offer a classification method, meaning an individual atom or shape is assigned to a tissue. In operation planning a sphere-filled organ modeling [28] can be found. This representation is close to voxels. But depending on the modeled anatomy, it is probably memory intense as no spheres inside an area can be omitted. Furthermore, it is possible to model single organ shapes via Fourier surfaces [29], spherical harmonics [30]–[32], and wavelets [33], [34]. These methods are not available in common software and have to be implemented by the user. They are based on a set of parameters and are not editable in a straightforward way via graphical interaction and require a specialist for applying. Further mathematical descriptions mainly describing the contour of an organ can be found in [35]–[38]. These approaches are commonly used for segmentation, i.e., organ extraction from medical images; to the authors' knowledge they are not used as input format for the simulation of radiation transport.

III. Conceptual Basics

For a single source point, analogous to an electric charge, the 3-D potential field in a homogeneous medium is a sphere, and if cut by any plane, the equipotential lines are circles. For a group of source points the superposition principle works, and the resulting equipotential line will form a more detailed contour, see Figs. 1 and 2.

It shall be analyzed if this idea can be put in praxis, and how the source points can be distributed to obtain a resulting equipotential line that is closely tracing a given realistic organ contour.

A. Source Points With (Q/r)-Potential

For a better understanding how the source points can lead to a contour a short derivation of the underlying electric field principle is presented here

$$\vec{E} = \frac{Q}{4\pi\varepsilon r^2}\vec{e}_r. \tag{1}$$

Formula (1) shows the electrical field strength $\vec{E}$ of an electrical point charge Q in a medium with the dielectric constant ε at a distance r. The associated electrical potential φ is

$$\varphi = \frac{Q}{4\pi\varepsilon r}. \tag{2}$$

For a distribution of z point charges the resulting electrical potential φ is obtained according to the superposition principle

$$\varphi = \sum_{i=0}^{z} \frac{Q_i}{4\pi\varepsilon r_i}. \tag{3}$$

In order to model the organ surfaces and no actual physical situation we use a mathematical analogy: we consider source points instead of electrical point charges. The physical constant ε is neglected, a "source strength" Q_i is associated with each source point i resulting in a sum potential φ. We define that Q_i is a positive number and r is the distance from the point source. The potential for a spatial distribution of z source points is

$$\varphi = \sum_{i=0}^{z} \frac{Q_i}{r_i}. \tag{4}$$

B. Computation and Display of the Potential-Based Lines

To show a line of equipotentials it is necessary to pick a field point and compare its local potential φ_0 to the rest of the potential field. It is the question how to decide for this point of reference. To answer this question the inertia axes of the organ slice were utilized.

The axes of inertia span a coordinate system with their origin in the barycenter B of the organ slice, as shown in Fig. 3. The axes cut the organ borders and the intersection points serve as reference for the potential. In the process

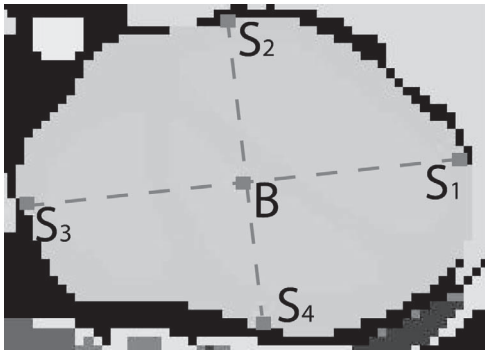

Fig. 3. Transversal voxelized slice of the heart with barycenter B and intersection points $S_{1...4}$ of the inertia axes and organ border.

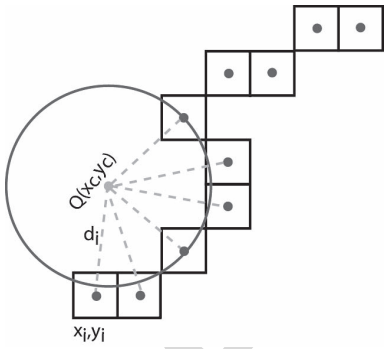

Fig. 4. Computation of source point coordinates x_c, y_c by circle approximation of x_j, y_j.

of first implementation the potential-based contours for all four intersection points $S_{1...4}$ were displayed and compared. The resulting potential-based contours are slightly different and shall be compared by parameters of goodness, see Section III-E.

C. Positioning of the Source Points

After the consideration how to adapt the basic idea and how to display a potential-based contour there is still the open question how many and where to place source points in a sensible way to proof the concept.

The already known organ border of a voxelized computational phantom shall serve as a guideline for the potential-based contours. The voxel model "Laura" [39] of the HMGU voxel model family [6] provided the organ borders that were transformed in potential-based contours. The so-called voxelized phantoms offer a realistic presentation of human anatomy. Here, it can be seen if the method of a source point distribution fits for realistic organ shapes. In essence every other phantom of [6] or set of contour coordinates could be used.

1) Coordinates of the Source Points: An iteration process shall distribute a number of sources within the given organ border. The individual source points have to be placed in regard to their respective border segment, which is obtained by dividing the total number of border voxels by the total number of sources. Since the equipotential line of a single source point is a circle in 2-D (see Section III, Fig. 1), it is assumed the respective border voxels x_j, y_j are on this circle and the source is placed at its center point x_c, y_c at a the radius r.

Formula (5) describes the variation of the center point coordinates and its distance to each border voxel x_j, y_j by means of auxiliary variables ϑ, η, ρ

$$(x_c, y_c, r) = \underset{\vartheta,\eta,\rho}{\operatorname{argmin}} \sum_{j=1}^{n} \left[\left(x_j - \vartheta\right)^2 + \left(y_j - \eta\right)^2 - \rho^2 \right]^2. \quad (5)$$

This algorithm serves to minimize the sum of the squared differences $(d_j^2 - r^2)^2$, where

$$d_j^2 = \left(x_j - x_c\right)^2 + \left(y_j - y_c\right)^2. \quad (6)$$

These expressions were the basis for a system of equations whose final matrix formulation was solved via Cramers' rule and thus provided the desired center points x_c, y_c.

D. Choice of the Source Strengths

After the source points Q_i have been placed in a distance r to the border, the source strengths are determined by

$$Q_i = r_i \cdot \varphi_R \quad (7)$$

where the potential on the border is $\varphi_R = 1$. The sum potential on the organ border φ_0 will differ from 1 because of the superposition of all point sources. It is expected to be higher but remaining within the same order of magnitude. Among all tried ways this simple one provided adequate results.

E. Comparison of the Potential-Based Organ Area With Voxel Area

After placing the source points and displaying the equipotential line there must be a way of judging how well the final potential-based contour matches the voxelized one. For this purpose the parameters of goodness are introduced.

1) Parameters for the Goodness of Fit: For the comparison of the equipotential with the voxel representation, the overlap U between the potential-modeled and originally voxelized organ region is computed. The combined area of voxelized (O) and potential-based (M) organ region except the intersection of both is related to the original region (O) by

$$U = \frac{O \cup M \setminus O \cap M}{O}. \quad (8)$$

This can be intuitively understood as organ area not covered by the potential-based region. The closer to zero the better the match between the areas. Because one goodness-of-fit parameter did not turn out to be sufficient, the distance a between the barycenters of original and potential-based contour were additionally calculated

$$a = \sqrt{(x_O - x_M)^2 + (y_O - y_M)^2}. \quad (9)$$

Formula (9) subtracts the coordinates (x_O, y_O) and (x_M, y_M) of the barycenters of the original and modeled area and a is given in voxel distances. The optimal case is when there is no distance between the barycenters, i.e., the expression is zero.

The values U and a are calculated for a source point distribution, the pair with the smallest values, i.e., closest to zero, indicates the best fit. This way resulting potential-based contours can be compared and evaluated.

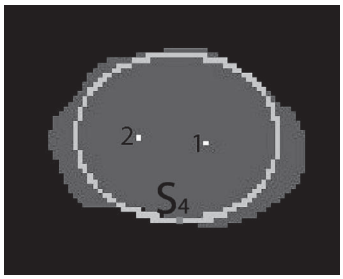

Fig. 5. Voxelized heart slice (dark gray) with potential-based contour (light gray) of 2Q, U=0.05, a=0.44, S_4.

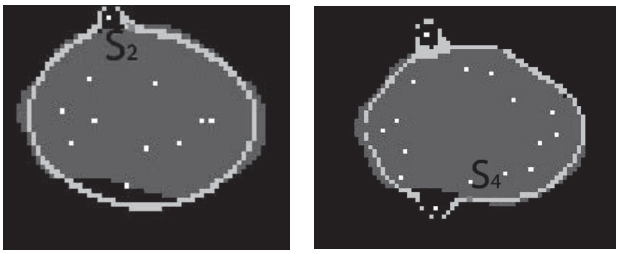

Fig. 6. Heart with 11Q (U=0.04, a=1.13, left) and 16 Q(U=0.04, $a = 0.71$, right).

IV. Results

The transversal slice T256 of the voxel data set Laura provided the heart contour that served for testing the new method, see Figs. 5–7. After the evaluation of the first trials, the positioning of the source points, see Section IV-B, was refined and applied for organ slices of heart, bladder, stomach, and aorta, as presented in Section IV-C.

A. First Trials

For the heart slice, the number of source points was varied from 2 to 42. The parameters of goodness U and a were analyzed for every distribution at the four intersection points S_1, S_2, S_3, or S_4 between the axes of inertia and the organ border. Table I shows an excerpt of the parameters for the iteration process. The full table can be found in [40].

For just two source points, Fig. 5 shows that the principle of superposition is working. Exact tracing of the organ contour is not yet achieved, but that a match between the equipotential line and the organ border appears as possible, when the number of source points is increased. The distributions with 11 sources (Fig. 6, left) and 16 sources (Fig. 6, right) show the best parameters of all distributions. For both approximations small areas outside the original organ contour have been modeled, this is due to the more concave segment of the organ contour, the single source was oriented to.

In the example of Fig. 7 the probable optimal number of source points is exceeded. Ring structures were created rather than a closed area.

B. Conclusion for Source Point Positioning

From these results the following conclusions have been deduced.

1) The algorithm for minimization the goodness-of-fit parameters does not have an unique solution. For one organ contour several source point distributions with nearly the same set of goodness parameters have been found.
2) Highly curved contours benefit from a higher number of source points.

The following rules for numerical stability were adopted in the placing algorithm.

1) In a distribution with source points of the same sign, the source points have to be placed inside the organ region.
2) Source points very close to or on the organ border lead to numerical instabilities. Improvements may be achieved by eliminating unfavorable source points.

TABLE I
Iterations of 9–18 Source Points Q, With the Goodness-of-Fit Parameters U and a for the Intersection Points S_1 to S_4

Q Number	S_i	U	a
9	S_1	0.05	1.47
9	S_2	0.05	1.65
9	S_3	0.07	1.31
9	S_4	0.07	2.25
10	S_1	0.05	1.97
10	S_2	0.05	1.99
10	S_3	0.05	2.14
10	S_4	0.1	2.36
11	S_1	0.06	1.19
11	S_2	0.04	1.13
11	S_3	0.05	1.18
11	S_4	0.09	1.09
12	S_1	0.08	8.27
12	S_2	0.08	7.32
12	S_3	0.1	9.02
12	S_4	0.13	8.76
13	S_1	0.07	3.59
13	S_2	0.08	3.34
13	S_3	0.1	3.13
13	S_4	0.08	3.81
14	S_1	0.07	2.07
14	S_2	0.07	2.26
14	S_3	0.1	2.3
14	S_4	0.09	3.23
15	S_1	0.07	8.35
15	S_2	0.06	7.92
15	S_3	0.07	8.22
15	S_4	0.06	7.33
16	S_1	0.04	1.3
16	S_2	0.04	0.96
16	S_3	0.05	0.24
16	S_4	0.04	0.71
17	S_1	0.04	4.21
17	S_2	0.04	4.73
17	S_3	0.05	4.54
17	S_4	0.05	5.02
18	S_1	0.13	4.28
18	S_2	0.07	4.99
18	S_3	0.08	4.95
18	S_4	0.09	5.44

Fig. 7. Heart T256 with 29 Q ($U = 0.18$, $a = 1.02$, left) and 39 Q (U=0.24 a=0.75, right) each for S_1.

C. Potential-Based Organ Contour

Based on this experience, potential-based contours for slices of heart, aorta, kidney, stomach, and bladder have

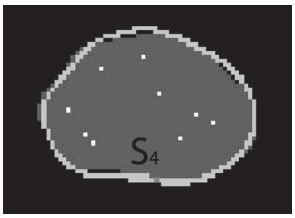

Fig. 8. Heart slice T256, 9 Q, $U = 0.02$, and $a = 0.29$ for S_4.

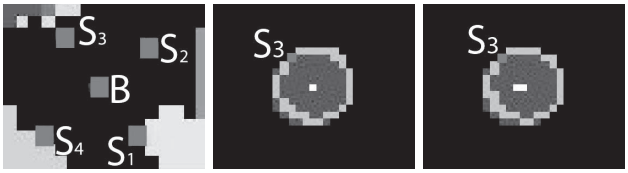

Fig. 9. Voxelized slice of aorta with barycenter B and intersections points $S_{1...4}$ (left) and potential-based contours with $1Q$ (middle) and $2Q$ (right), both $U = 0.04$, $a = 0.02$ for S_3.

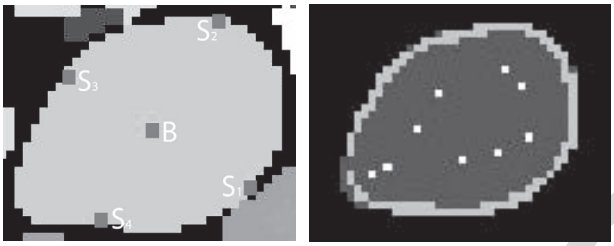

Fig. 10. Voxelized kidney slice with barycenter B and intersections points$S_{1...4}$ (left) and $9Q$, $U = 0.01$, and $a = 0.55$ for S_1 (right).

been generated. The source points were distributed within the organ region but neither close nor on the organ border according to the numerical stability rules of the placing algorithm.

Figs. 8–12 present the original voxelized slices together with the best source point distributions with their respective goodness parameters. The area within and including the potential-based contour can be understood as organ area.

1) Heart, Aorta, and Kidney: After the implementation of the restrictions for placing the sources a distribution of nine sources provided the best fit of the potential and voxel-based contour for the heart slice (Fig. 8).

For the aorta the distribution of one and two source points worked the same because of its nearly circular shape. For radiation protection purposed the aorta is not divided in wall and blood volume.

The best set of parameters of all organs has been achieved for the kidney (Fig. 10). Only very few voxels were found outside the equipotential line.

2) Walled Organs: In the underlying voxel data of stomach (Fig. 11) and bladder (Fig. 12) consist of wall and content. Here, the content provided the coordinates for the source point placement.

In the upper part of Fig. 11 the equipotential line of seven source points covers a small area outside the organ.

Similar to the stomach, the bladder (Fig. 12) is divided in wall and content. Here, too the content was taken as basis for the source point placements.

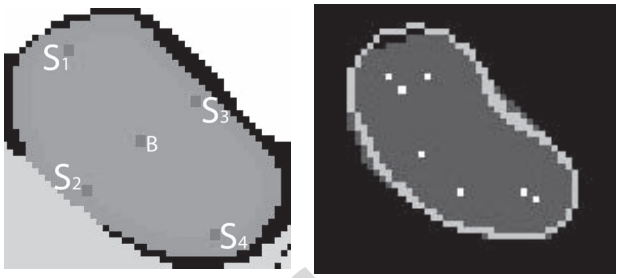

Fig. 11. Stomach T250, B and $S_1..S_4$ (left); $7Q$, $U = 0.02$, and $a = 0.21$ for S_4 (right).

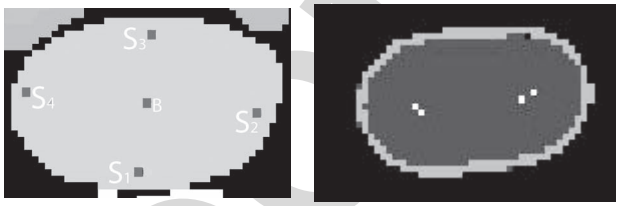

Fig. 12. Bladder T185, B, and $S_{1...4}$ (left); 4 Q, $U = 0.02$, and $a = 0.27$ for S_1 (right).

V. Discussion of Potential-Based Features

Figs. 8–12 give proof the principle of source points works and show that a satisfying quality of modeling is achieved; even slightly concave contours were modeled by the proper choice of source distances.

A. Data Compression

For saving a continuous contour the coordinates of the source points and the potential value at the respective reference point are needed, for the given examples it was less than 12 numbers. The calculation time for obtaining a distribution for a given number of source points is in the range of a few seconds.

B. Data Input for Source Point Placing

Since the data for the center calculations are coordinates, the algorithm works for coronal, sagittal, and transversal slices. The results of Section IV were obtained by implementing the voxel model Laura [39]. The method can be applied also to other voxel phantoms. To demonstrate this, heart contours of the human phantoms Golem (T55 $U = 0.02$, $a = 0.13$) and Irene (T255 $U = 0.02$, $a = 0.55$) were modeled. In theory also other boundary representations, such as polygon meshes, could deliver the basis coordinates for positioning the source points as long as the boundary contour can be approximated by circles (2-D) or spheres (3-D).

C. Scaling

A potential-based organ contour can be easily scaled in size. It is sufficient to multiply the coordinates of the source points as well as their source strengths Q_i by a factor s. For the enlarged heart region, shown in Fig. 13, a factor $s = 1.4$ was

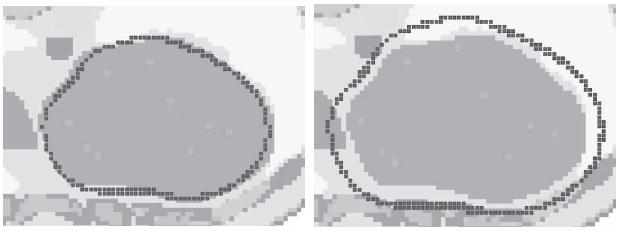

Fig. 13. Scaling of the equipotential line $\varphi_0 = 4.13$ (red) in the heart slice T256 (brown).

chosen arbitrarily

$$\varphi_{\mathbf{0}} = \sum_{i=0}^{z} \frac{sQ_i}{sr_i} = \sum_{i=0}^{z} \frac{Q_i}{r_i}. \tag{10}$$

Although all coordinates will be subjected to this affine transformation, the potential φ_0 on the equipotential line will be conserved.

This feature is of interest when existing organ model have to be adapted to individual shapes of a patient. For this purpose also a change of place and source strength of the single sources is of interest if a rigid transformation is not sufficient. At the moment this feature works only manually.

D. Walled Organs and Subtissue

It is possible to describe the organ wall as a potential range, e.g., $\varphi_{\text{wall}} = \varphi_0 \pm \Delta\varphi$. For subtissues inside an organ a range of potential values could be utilized. In a voxel model all voxel adjacent to another tissue make the organ border. It is straightforward that the resolution of the voxels influence the resulting thickness of the wall. In this case Laura provides voxels of $1.875 * 1.875 * 5$ mm^3 which makes it difficult to present walled or thin organs in a accurate way.

E. In- or Outside Criterion of the Potential-Based Contour

For a Monte Carlo simulation of radiation transport the released energy of an interaction has to be assigned to an organ volume. In case of a voxelized human phantom the organ identification number of a specific voxel informs about the tissue type. In case of boundary representations like polygon meshes and NURBS there is no according information. It is possible to implement these type of phantoms to Monte Carlo code but it is computational intense [41]. Additional algorithms deliver spatial information for assigning the released energy to the correct corresponding tissue, i.e., within which organ contour energy loss happens, [42].

The equipotential line is a closed continuous contour, suitable for compact organs like heart, bladder, or stomach, whose surfaces primarily show convex regions. To check where an arbitrary point is situated in respect to the organ border, it is sufficient to see if $\varphi > \varphi_0$ for being inside or $\varphi < \varphi_0$ for being outside. Further studies are necessary to show if the potential values and the gradient of the potential field provide the expected benefits.

VI. Conclusion

The first trials of the newly explored method of potential-based organ contours look promising and provide further aspects for development. The organ contours were modeled by a source point distribution with an $(1/r)$-potential. This physical approach offers an advantage by making use of the inherent features of the physical quantities and the connections among each other. This way a potential-based delineation provides more information about the organ shape despite basing on a small data set. It offers a flexible frame for delineate natural contours. Depending on the complexity of the organ, a point source might not provide an adequate field geometry. Further studies with other sources, e.g., a line source, would be needed. The regulation of the individual source strengths is a complex issue. The alteration of a single source strength is affecting the whole field and changes the resulting equipotential line.

The focus of this paper was on compact mostly convex organ shapes in 2-D to proof the principle. For small concave parts of organ contours have been satisfactorily modeled by proper spacing between positive sources. The developed placing algorithm is rather basic and does not deliver satisfying results for organ contours with more convex parts or peaks, e.g., tips of the lungs. These parts would benefit from negative sources.

The proposed method can further be used for the extraction of organs from medical images, i.e., for their segmentation. Therefore, a first guess of the contour has to be placed into the medical image. This can be done either manually by placing sources with the mouse or taken from an already voxelized organ border. Here, the implied features of the physical approach are used, i.e., electric force and the field lines of the sources pointing in radial direction away. In combination with an edge detection of the medical image, the field lines of a source and the gradient of the edges are used to tell how well a source point is oriented toward the respective edge. The source points can be shifted individually in a predefined area to a place where the resulting equipotential line traces the edge in a better way. First tests on CT-images with practical results have been made [40].

Outlook

It would be interesting to try more advanced algorithms for source point positioning and the calculation of the source strengths, as well as other potential distributions that may offer mathematical advantages or face special needs for contouring. The implementation of negative source points is an aspects which should be addressed. Concave sections of the organ border would benefit from the use of negative sources.

The implementation of the potential-based method into Monte Carlo simulations of radiation transport is considered possible, see Section V-E. Small and thin walled organs could be represented which have not been included in Monte Carlo code until now. The point of data compression is also interesting in regard to the computationally intense simulation of radiation transport. Therefor, a 3-D representation with sources is necessary. Equations (5) and (6) were also extended to 3-D but not yet implemented. The compact data structure of the potential-based organ contours also appears applicable in computer assisted diagnosis and growth modeling for tumors, e.g., in brains or tumor or organ tracking in radiation therapy.

ACKNOWLEDGMENT

The authors would like to thank the Technische Universität Ilmenau and the Helmholtz Zentrum München, especially Prof. A. Keller and Prof. D. Regulla, for the possibility to do this paper and the provided support. Furthermore, the authors would also like to express my sincere gratitude to my advisor Prof. D. Harder, Universität Göttingen, for his support and guidance.

REFERENCES

[1] M. Bro-Nielsen, "Finite element modeling in surgery simulation," *Proc. IEEE*, vol. 86, no. 3, pp. 490–503, Mar. 1998.

[2] T. Nagaoka *et al.*, "Development of realistic high-resolution whole-body voxel models of Japanese adult males and females of average height and weight, and application of models to radio-frequency electromagnetic-field dosimetry," *Phys. Med. Biologie*, vol. 49, no. 1, pp. 1–15, 2004.

[3] P. Dimbylow, "Development of the female voxel phantom, NAOMI, and its application to calculations of induced current densities and electric fields from applied low frequency magnetic and electric fields," *Phys. Med. Biol.*, vol. 50, no. 6, pp. 1047–1070, 2005.

[4] M. Clemens *et al.*, "Bioelectromagnetic field simulations using high-resolution human anatomy models with the finite integration technique," *J. RF Eng. Telecommun.*, vol. 63, nos. 7–8, pp. 163–167, 2009.

[5] W. Bolch, C. Lee, M. Wayson, and P. Johnson, "Hybrid computational phantoms for medical dose reconstruction," *Radiat. Environ. Biophys.*, vol. 49, no. 2, pp. 155–168, 2010.

[6] N. Petoussi-Henss, M. Zankl, U. Fill, and D. Regulla, "The GSF family of voxel phantoms," *Phys. Med. Biol.*, vol. 47, no. 1, pp. 89–106, 2002.

[7] R. Kramer, J. W. Vieira, H. J. Khoury, F. R. A. Lima, and D. Fuelle, "All about MAX: A male adult voxel phantom for Monte Carlo calculations in radiation protection dosimetry," *Phys. Med. Biol.*, vol. 48, no. 10, pp. 1239–1262, 2003.

[8] R. Kramer *et al.*, "All about FAX: A female adult voxel phantom for Monte Carlo calculation in radiation protection dosimetry," *Phys. Med. Biol.*, vol. 49, no. 23, pp. 5203–5216, 2004.

[9] C. Y. Shi and X. G. Xu, "Development of a 30-week-pregnant female tomographic model from computed tomography (CT) images for Monte Carlo organ dose calculations," *Med. Phys.*, vol. 31, no. 9, pp. 2491–2497, 2004.

[10] S. Park, J. K. Lee, and C. Lee, "Development of a Korean adult male computational phantom for internal dosimetry calculation," *Radiat. Protect. Dosimetry*, vol. 121, no. 3, pp. 257–264, 2006.

[11] K. Sato, H. Noguchi, Y. Emoto, S. Koga, and K. Saito, "Japanese adult male voxel phantom constructed on the basis of CT images," *Radiat. Protect. Dosimetry*, vol. 123, no. 3, pp. 337–344, 2007.

[12] B. Zhang, J. Ma, L. Liu, and J. Cheng, "CNMAN: A Chinese adult male voxel phantom constructed from color photographs of a visible anatomical data set," *Radiat. Protect. Dosimetry*, vol. 124, no. 2, pp. 130–136, 2007.

[13] B. He *et al.*, "Grand challenges in interfacing engineering with life sciences and medicine," *IEEE Trans. Biomed. Eng.*, vol. 60, no. 3, pp. 589–598, Mar. 2013.

[14] F. Spiers, "Transition-zone doesimetry," in *Radiation Protection Dosimetry*, F. H. Attix and E. Tochilin, Eds., vol. 3. New York, NY, USA: Academic Press, 1968, pp. 809–867.

[15] "Adult reference computational phantoms," *Ann. ICRP*, vol. 39, no. 2, pp. 1–2, 2009.

[16] H. L. Fisher and W. S. Snyder, "Distribution of dose in the body from a source of gamma rays distributed uniformly in an organ," Oak Ridge Nat. Lab., Oak Ridge, TN, USA, Rep. ORNL 4168, 1967.

[17] R. Kramer, M. Zankl, G. Williams, and G. Drexler, "The calculation of dose from external photon exposures using reference human phantoms and Monte Carlo methods, part I: The male (Adam) and female (Eva) adult mathematical phantoms," GSF-Nat. Res. Center Environ. Health, Rep. GSF S-885, 1982.

[18] M. Cristy and K. F. Eckerman, "Specific absorbed fractions of energy at various ages from internal photon sources," Oak Ridge Nat. Lab., Oak Ridge, TN, USA, Rep. ORNL TM-8381, 1987.

[19] J. Becker, M. Zankl, and N. Petoussi-Henss, "A software tool for modification of human voxel models used for application in radiation protection," *Phys. Med. Biol.*, vol. 52, no. 9, pp. 195–205, 2007.

[20] X. G. Xu, V. Taranenko, J. Zhang, and C. Shi, "A boundary-representation method for designing whole-body radiation dosimetry models: Pregnant females at the ends of three gestational periods—RPI-P3, -P6 and -P9," *Phys. Med. Biol.*, vol. 52, no. 23, pp. 7023–7044, 2007.

[21] C. Lee, C. Lee, S.-H. Park, and J.-K. Lee, "Development of the two Korean adult tomographic computational phantoms for organ dosimetry," *Med. Phys.*, vol. 33, no. 2, pp. 380–390, 2006.

[22] C. Lee *et al.*, "The UF family of reference hybrid phantoms for computational radiation dosimetry," *Phys. Med. Biol.*, vol. 55, no. 2, pp. 339–363, 2010.

[23] J. Bond *et al.*, "Series of 4D adult XCAT phantoms for imaging research and dosimetry," in *Proc. SPIE*, vol. 8313, 2012, Art. no. 83130P.

[24] C. H. Kim *et al.*, "The reference phantoms: Voxel vs polygon," *Ann. ICRP*, vol. 45, no. S1, pp. 188–201, 2016.

[25] B. Tsagaan, A. Shimizu, H. Kobatake, and K. Miyakawa, *An Automated Segmentation Method of Kidney Using Statistical Information* (Lecture Notes in Computer Science), vol. 2488. Heidelberg, Germany: Springer, 2002, pp. 556–563, doi: 10.1007/3-540-45786-0_69.

[26] (2015). *Rhinoceros—NURBS Modeling Für Windows, Version 4 SR9, 9-March-2011 Commercial*. [Online]. Available: https://www.flexicad.com/

[27] H. Blum, "Biological shape and visual science (part I)," *J. Theor. Biol.*, vol. 38, no. 2, pp. 205–287, 1973.

[28] S. Suzuki, N. Suzuki, A. Hattori, A. Uchiyama, and S. Kobayashi, "Sphere-filled organ model for virtual surgery system," *IEEE Trans. Med. Imag.*, vol. 23, no. 6, pp. 714–722, Jun. 2004.

[29] L. H. Staib and J. S. Duncan, "Deformable Fourier models for surface finding in 3-D images," *Visual. Biomed. Comput.*, vol. 1808, pp. 90–104, 1992.

[30] F. Mofrad *et al.*, "Statistical construction of a Japanese male liver phantom for internal radionuclide dosimetry." *Radiat. Protect. Dosimetry*, vol. 141, no. 2, pp. 140–148, 2010.

[31] T. Tateyama *et al.*, "Shape representation of human anatomy using spherical harmonic basis function," in *Proc. 6th Int. Conf. Comput. Sci. Converg. Inf. Technol. (ICCIT)*, 2011, pp. 866–869.

[32] A. Matheny and D. B. Goldgof, "The use of three- and four-dimensional surface harmonics for rigid and nonrigid shape recovery and representation," *IEEE Trans. Pattern Anal. Mach. Intell.*, vol. 17, no. 10, pp. 967–981, Oct. 1995.

[33] C. Davatzikos, X. Tao, and D. Shen, "Hierarchical active shape models, using the wavelet transform," *IEEE Trans. Med. Imag.*, vol. 22, no. 3, pp. 414–423, Mar. 2003.

[34] D. Nain, S. Haker, A. Bobick, and A. Tannenbaum, "Multiscale 3-D shape representation and segmentation using spherical wavelets," *IEEE Trans. Med. Imag.*, vol. 26, no. 4, pp. 598–618, Apr. 2007.

[35] C. Xu and J. L. Prince, "Snakes, shapes, and gradient vector flow," *IEEE Trans. Image Process.*, vol. 7, no. 3, pp. 359–369, Mar. 1998.

[36] T. McInerney and D. Terzopoulos, "A dynamic finite element surface model for segmentation and tracking in multidimensional medical images with application to cardiac 4D image analysis," *Comput. Med. Imag. Graph.*, vol. 19, no. 1, pp. 69–83, 1995.

[37] D. Cremers, M. Rousson, and R. Deriche, "A review of statistical approaches to level set segmentation: Integrating color, texture, motion and shape," *Int. J. Comput. Vis.*, vol. 72, no. 2, pp. 195–215, 2007.

[38] T. Heimann and H.-P. Meinzer, "Statistical shape models for 3D medical image segmentation: A review," *Med. Image Anal.*, vol. 13, no. 4, pp. 543–563, 2009.

[39] M. Zankl, K. F. Eckerman, and W. Bolch, "The ICRP reference computational phantoms," *Handbook of Anatomical Models for Radiation Dosimetry*. Boca Raton, FL, USA: Taylor & Francis, 2010, pp. 377–388.

[40] J. Becker, "Beschreibung von organgrenzen als Äquipotentialverlauf finiter quellpunkte mit Q/r-potentialen," Ph.D. Dissertation, Technische Universität Ilmenau, Ilmenau, Germany, 2015.

[41] C. H. Kim, J. J. H. W. Bolch, K. K. Cho, and S. B. Hwang, "A polygon-surface reference Korean male phantom (PSRK-Man) and its direct implementation in Geant4 Monte Carlo simulation," *Phys. Med. Biol.*, vol. 56, no. 10, pp. 3137-3161, 2011.

[42] M. Han *et al.*, "DagSolid: A new Geant4 solid class for fast simulation in polygon-mesh geometry." *Phys. Med. Biol.*, vol. 58, no. 13, pp. 4595–4609, 2013.

AUTHOR QUERIES

AUTHOR PLEASE ANSWER ALL QUERIES

PLEASE NOTE: We cannot accept new source files as corrections for your paper. If possible, please annotate the PDF proof we have sent you with your corrections and upload it via the Author Gateway. Alternatively, you may send us your corrections in list format. You may also upload revised graphics via the Author Gateway.

AQ1: Please provide the postal code for "AMSD—Research Unit Medical Radiation Physics and Diagnostics."
AQ2: Please cite "Fig. 4" inside the text.
AQ3: Please provide the author name for Reference [15].
AQ4: Please provide the organization location for Reference [17].
AQ5: Please confirm if the location and publisher information for Reference [25] is correct as set.
AQ6: Please confirm the volume number for References [23] and [25].
AQ7: Please confirm the volume number and also provide the issue number or month for Reference [29].
AQ8: Please provide the department name for Reference [40].